TISSUE ENGINEERING: Part A
Volume 19, Numbers 15 and 16, 2013

DOI: 10.1089/ten.tea.2012.0520

Titanium-Enriched Hydroxyapatite–Gelatin Scaffolds with Osteogenically Differentiated Progenitor Cell Aggregates for Calvaria Bone Regeneration

João R. Ferreira, DDS, PhD,[1,2] Ricardo Padilla, DDS,[2] Ganokon Urkasemsin, DVM, PhD,[3,4] Kun Yoon,[2] Kelly Goeckner, DDS,[2] Wei-Shou Hu, PhD,[5] and Ching-Chang Ko, DDS, PhD[2,6]

Adequate bony support is the key to re-establish both function and esthetics in the craniofacial region. Autologous bone grafting has been the gold standard for regeneration of problematic large bone defects. However, poor graft availability and donor-site complications have led to alternative bone tissue-engineering approaches combining osteoinductive biomaterials and three-dimensional cell aggregates in scaffolds or constructs. The goal of the present study was to generate novel cell aggregate-loaded macroporous scaffolds combining the osteoinductive properties of titanium dioxide (TiO_2) with hydroxyapatite–gelatin nanocomposites (HAP-GEL) for regeneration of craniofacial defects. Here we investigated the *in vivo* applicability of macroporous (TiO_2)-enriched HAP-GEL scaffolds with undifferentiated and osteogenically differentiated multipotent adult progenitor cell (MAPC and OD-MAPC, respectively) aggregates for calvaria bone regeneration. The silane-coated HAP-GEL with and without TiO_2 additives were polymerized and molded to produce macroporous scaffolds. Aggregates of the rat MAPC were precultured, loaded into each scaffold, and implanted to rat calvaria critical-size defects to study bone regeneration. Bone autografts were used as positive controls and a poly(lactic-co-glycolic acid) (PLGA) scaffold for comparison purposes. Preimplanted scaffolds and calvaria bone from pig were tested for ultimate compressive strength with an Instron 4411® and for porosity with microcomputerized tomography (μCT). Osteointegration and newly formed bone (NFB) were assessed by μCT and nondecalcified histology, and quantified by calcium fluorescence labeling. Results showed that the macroporous TiO_2-HAP-GEL scaffold had a comparable strength relative to the natural calvaria bone (13.8 ± 4.5 MPa and 24.5 ± 8.3 MPa, respectively). Porosity was 1.52 ± 0.8 mm and 0.64 ± 0.4 mm for TiO_2-HAP-GEL and calvaria bone, respectively. At 8 and 12 weeks postimplantation into rat calvaria defects, greater osteointegration and NFB were significantly present in the TiO_2-enriched HAP-GEL constructs with OD-MAPCs, compared to the undifferentiated MAPC-loaded constructs, cell-free HAP-GEL with and without titanium, and PLGA scaffolds. The tissue-engineered TiO_2-enriched HAP-GEL constructs with OD-MAPC aggregates present a potential useful therapeutic approach for calvaria bone regeneration.

Introduction

Craniofacial bone is essential in providing protection for internal organs (brain), and support for facial soft tissues. Annually, 2.3 million excision procedures for bone graft replacement are performed. Craniofacial surgical procedures are among the most common regenerative procedures.[1] Major conventional substitutes for bone replacement in the craniofacial region include autogenous, allogeneic, and alloplastic or synthetic grafts. Autogenous grafts are well-known clinical gold standards; however, complications from donor excision sites may arise, as well as poor availability to repair large defects and lack of formability (ability to shape to a defect).[2] Secondly, allogeneic grafts from freeze-dry bone banks present immunogenic risks and are devoid of a cell reservoir that contributes to the formation of new bone.[3,4] These limitations increased the focus of bioengineers on alloplastic grafts.[3,4]

[1]National Institute of Dental and Craniofacial Research, Bethesda, Maryland.
[2]School of Dentistry, University of North Carolina-Chapel Hill, Chapel Hill, North Carolina.
[3]Department of Pre-Clinical and Applied Animal Sciences, Faculty of Veterinary Science, Mahidol University, Phutthamonthon, Thailand.
[4]College of Veterinary Medicine, North Carolina State University, Raleigh, North Carolina.
[5]Chemical Engineering and Materials Science, University of Minnesota, Minneapolis, Minnesota.
[6]Material Sciences and Engineering, North Carolina State University, Raleigh, North Carolina.

The purpose of this study was to investigate whether hydroxyapatite–gelatin (HAP-GEL) alloplastic materials can be used as a bone replacement porous scaffold/construct to carry three-dimensional (3D) cell aggregates.[5] HAP-GEL cross-linked with an aminosilane was previously found to exhibit an appropriate compressive strength (100 MPa), biocompatibility and facilitate surface bone ingrowth.[6,7] The loading of cells on alloplastic grafts such as porous calcium-based scaffolds in the hydroxyapatite form (HAP), followed by *in vivo* implantation in large bone defects, had been previously shown to promote healing.[8,9] Moreover, injectable and formable calcium-based composites with natural polymeric phases (e.g., gelatin) can further increase their clinical applicability.[10]

Titania additives may constitute an advantage by increasing surface hydrophobicity and protein adsorption to further enhance cell adhesion, osteogenic induction, and formability in bone biomaterials, including in HAP-GEL.[7,11,12] Consequently, bone regeneration of formable titanium dioxide (TiO_2)-enriched HAP-GEL scaffolds was compared in this study to HAP-GEL alone.

HAP-based scaffolds have been successfully combined with stem cells to shorten the *in vivo* bone-healing time when compared to cell-free HAP.[5,13] Porous HAP-GEL scaffolds loaded with multipotent adult progenitor cells (MAPCs), a subpopulation of cells isolated from rat bone marrow, have recently been implanted *in vivo* in large bone defects. The construct was shown to be feasible to carry these MAPCs in 3D aggregates.[5] MAPCs hold important advantages over mesenchymal stem cells (MSC) in terms of homogeneity of surface markers.[14,15] They also have high levels of the Oct4 transcription factor, a high growth rate, and are able to be grown as 3D aggregates.[16,17] MAPCs are also capable of forming the three germ lineages, including the mesoderm that gives rise to bone tissue when dexamethasone is supplemented.[18,19] Recent studies demonstrate that clinical grade human MAPCs (Multistem®) offer clinical relevance for the treatment of autoimmune disorders and cardiac infarction (ClinicalTrials.gov NCT00677859, NCT00677222); however, no *in vivo* applicability studies for bone regeneration have been reported.

Here we report an *in vivo* MAPC-based bone regeneration model employing a novel 3D aggregate culture system, recently shown by our group to promote *in vitro* osteogenic differentiation.[5] To study the *in vivo* applicability of MAPC aggregates in macroporous constructs, we evaluated whether TiO_2-enriched HAP-GEL scaffolds loaded with MAPC 3D aggregates increase bone regeneration when compared to unloaded scaffolds. Since osteogenically differentiated cells may generate more newly formed bone (NFB) than uncommitted progenitor cells,[5,20] we tested whether rigid scaffolds with osteogenically differentiated MAPC (OD-MAPCs) aggregates produce more new bone than scaffolds with undifferentiated MAPCs. To accomplish these aims, a critical-size defect (CSD) model in rat calvaria was used to implant different HAP-GEL/MAPC constructs.

Materials and Methods

Fabrication of HAP-GEL macroporous scaffolds for calvaria defects

The HAP-GEL biomaterial was fabricated using biomimetic synthesis as described in previous studies.[6,7,21] Briefly, the HAP coprecipitation reaction was induced at 38°C in soluble GEL titrated with the $Ca(OH)_2$ solution. After the coprecipitation, the slurry was centrifuged and the supernatant removed. The condensed HAP-GEL slurry was then washed. The HAP-GEL precipitant was lyophilized and crosslinked with 11% weight enTMOS (bis[3-(trimethoxysilyl)-propyl]ethylenediamine). Phosphate-buffered saline 1×(16% of total weight) was added to confer injectability properties to the final HAP-GEL. Next, the HAP-GEL paste was loaded into a 1 cc syringe with a nasal diameter of 1 mm. To fabricate the dorsal cap that will hold the porous phase (Fig. 1), the paste was packed into a 12.7×2 mm cylindrical custom-made polypropylene mold. To develop the porous phase, the HAP-GEL paste was injected without packing in a spaghetti form over the dorsal cap to generate the macroporosity for cell retention and growth (Fig. 1). The scaffold was allowed to solidify, and then sent for gas sterilization. To fabricate TiO_2-enriched HAP-GEL scaffolds, a similar procedure was followed, but this time, TiO_2 (Evonik Aeroxide® P25) was added to the HAP-GEL (at silica:titanium atomic ratio of 60:40) before molding, as reported previously.[5,7]

Porosity of HAP-GEL scaffolds

HAP-GEL scaffolds (8 mm diameter×3 mm thickness) with and without titania, and same-size specimens from natural calvaria bone from pig were scanned and evaluated by microcomputed tomography (μCT). The μCT scanning was performed with a Portable Skyscan 1074 μCT System (Micro Photonics). The X-ray parameters were 40 kV at 1 mA with 420 ms-exposure time, and a spatial resolution of ~22 μm. The image matrix size was 768×576 pixels with acquired 2000 projections over a 360° rotation. All samples were positioned and scanned in a standard manner using an air-tight cylindrical sample holder. For the analysis of the acquired images, the CTAn analyser software (Micro Photonics) was used to measure the mean pore size. ImageJ software (NIH) was used to determine the scaffold and bone specimen porosity fraction (in%). Five specimens were analyzed for each HAP-GEL scaffold group (with and without titania).

Mechanical testing of HAP-GEL scaffolds

For compressive testing, macroporous HAP-GEL scaffolds with and without titania (8×3 mm) were compared to the

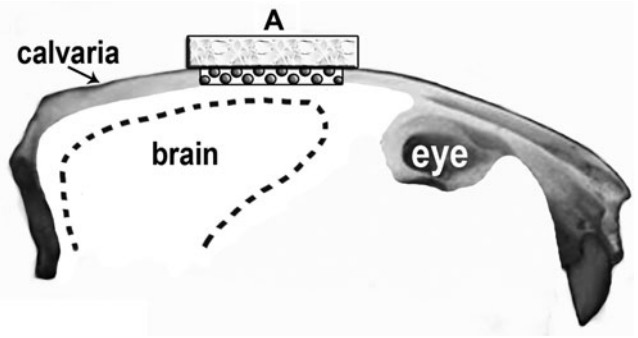

FIG. 1. Schematic representation of the macroporous and solid components of the hydroxyapatite–gelatin (HAP-GEL) scaffold **(A)** implanted in the 8-mm-critical-size defect (CSD) in rat calvaria.

same size: (1) natural calvaria bone specimens from pig and (2) porous collagen scaffolds (Nitta Gelatin, Inc.). All samples were compressed using an Instron® 4411 (Instron Co.) at 0.5 mm/min to determine the ultimate compressive strength. Five specimens were analyzed per group.

Aggregate MAPC culture, viability, and osteogenic differentiation

Rat MAPCs were isolated from bone marrow and were depleted of CD45 and Ter119 after 4 weeks in hypoxia culture conditions using magnetic microbeads and the remaining cells were seeded. After 3–14 weeks, cells with a typical spindle-shaped MAPC morphology appeared. Hypoxia conditions (incubator at 37°C with 5% O_2 and 5%–6% CO_2) were used to optimize MAPC expansion. To confirm that these clones were in fact MAPCs, the level of Oct4 mRNA was determined using quantitative real-time polymerase chain reaction and the presence of CD31, typical for MAPCs, was analyzed by fluorescence-activated cell sorting. Once a cell line with the MAPC phenotype (Oct4 mRNA at ΔCT of 4–6, and $CD31^+$) was derived, a large frozen working cell bank was prepared. The characteristics of the putative MAPCs were then evaluated (endothelial, hepatocyte, and neural precursor-like differentiation, and further transcriptome phenotype) as described previously.[15,17] During subsequent cell expansion, quality control studies were performed up to passage 30. Rat MAPCs from passage 20 were used for all the experiments of this study.

When osteogenic differentiation media were supplemented, cell cultures were changed to normal O_2 levels. For the 3D aggregate system, $1–2\times10^3$ MAPCs were seeded in suspension with the MAPC growth medium in 96-well-rounded bottom ultralow attachment plates (Costar #7007; Corning, Inc. Life Sciences), using a modification of a forced aggregation method previously reported.[5,17] The well plates were centrifuged to allow cells to settle to the bottom of the well and form aggregates over time. Aggregates were allowed to grow for 4 days in growth media, and then 10 undifferentiated aggregates were transferred and loaded into HAP-GEL scaffolds. Cell viability was assessed before *in vivo* implantation. A Live/Dead® Cell Vitality Assay kit (L34951; Molecular Probes) was used to confirm cell-active metabolism and viability according to the manufacturer's instructions. Metabolically active cells stained red fluorescent, and dead cells stained green. Fluorescence was visualized by microscopy with a Nikon Eclipse *Ti-U* with a digital camera, and Nikon NIS Elements software was used to render images (Nikon).

To generate OD-MAPCs, the MAPC osteogenic differentiation process was initiated *in vitro* by transferring 10 undifferentiated 3D aggregates to each well on 24-well ultralow attachment plates (Costar) with the osteogenic medium with dexamethasone. This 3D culture system and medium have been previously confirmed in our recent studies to be effective for MAPC osteogenic differentiation.[5] The osteogenic medium was composed of the MAPC basal medium with the addition of 10 mM of β-glycerophosphate (Sigma), ascorbic acid at 0.2 mM (Sigma), and dexamethasone at 10^{-7} M (Sigma).[15] The medium was changed every 2–3 days. The MAPCs were cultured for 38 days, and osteogenic differentiation was confirmed by (1) evaluating *in vitro* mineralization with crystal nucleation/formation in matrices by transmission electron microscopy (TEM); (2) assessing the formation of mineralized nodules with Alizarin Red; and (3) the presence of bone-specific markers (collagen type I, osteopontin, and osteocalcin) by immunohistochemistry in cryosectioned cell aggregate matrices, as previously described.[5] Then, 10

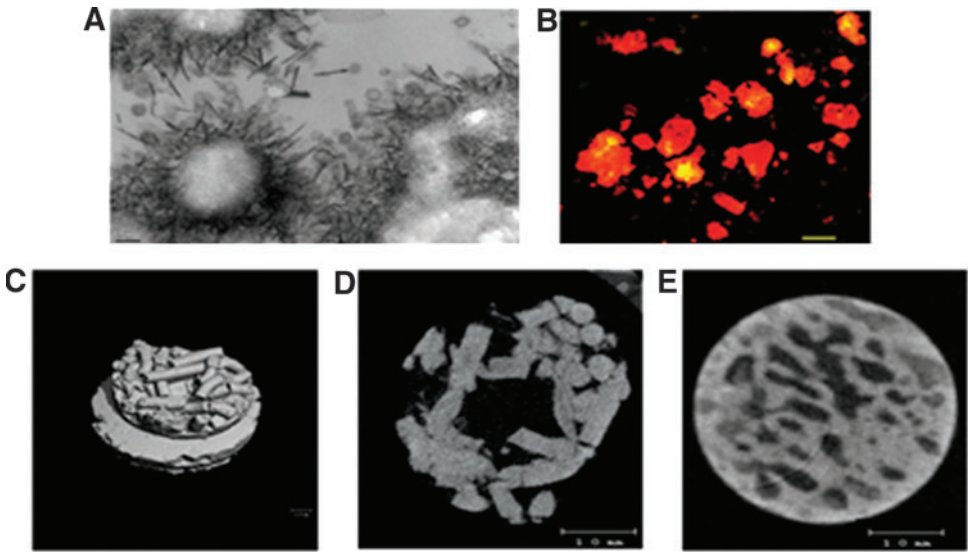

FIG. 2. Electron and fluorescence microscopy and microcomputerized tomography (μCT) images of osteogenically differentiated multipotent adult progenitor cell (OD-MAPC) aggregates/matrices and scaffolds. Top panel: *In vitro* mineralization of OD-MAPC aggregates/matrices seen in transmission electron microscopy (TEM) preimplantation **(A)** and cell viability of aggregates after transferring into macroporous HAP-GEL scaffolds **(B)**. Bottom panel: three-dimensional (3D) μCT image of the macroporous HAP-GEL scaffolds **(C)**, and μCT images comparing the porosity of macroporous HAP-GEL scaffolds **(D)** with calvaria natural bone **(E)** 2D cross sections. **(A)** TEM Mag.: 80,000×; **(B)** viable cells: red; nonviable cells: green-yellow; scale bar is 200 μm; Mag.: 100×; **(C–E)**: scale bar is 1.0 mm. Color images available online at www.liebertpub.com/tea

osteogenically differentiated aggregates from culture day 38 were loaded into the macroporous TiO_2-HAP-GEL scaffolds.

In vivo *implantation of macroporous HAP-GEL scaffolds with MAPC aggregates*

Craniofacial defects consisted of 8-mm-diameter calvaria CSD (Fig. 1), which have been previously described.[22–24] Briefly, 11- to 13-week-old Sprague-Dawley rats (Charles River) were anesthetized and a CSD was created on the calvaria bone using a dental trephine drill. Calvaria defects were assigned to the following experimental groups listed in Table 1. Porous collagen and poly(lactic-co-glycolic acid) (PLGA) scaffolds (Nitta Gelatin, Inc.) were used in this study as gold standard controls since both have been routinely placed to regenerate craniofacial and other orthopedic defects.[1–3,25,26] The sample size per group was equal to three. Two fluorochrome dyes were administered to evaluate the impact of different scaffolds on bone-healing rates[27]: (1) Alizarin Red S 30 mg/kg, (2) calcein, 20 mg/kg. Fluorochromes were administered to each animal by perivascular injection. Each rat received labels twice during the study. The first label (Alizarin Red) was given 10 days after the surgery, and the second (calcein) was given 15 days before sacrifice. There were interlabeling periods of 10 and 42 postsurgical days for rats sacrificed at 8 weeks and 10 and 70 days for the ones sacrificed at 12 weeks. After animals were euthanized (4, 8, and 12 weeks after surgery), calvaria specimens were placed in 10% formalin for 7 days, and then transferred to 70% isopropanol for μCT scanning.

μCT of surgical specimens

The μCT scanning (Scanco Medical μCT 40) was performed. The X-ray parameters were 70 kVp at 114 μA with a 200 ms integration time. The image matrix size was 2048×2048 with acquired 2000 projections over a 360° rotation. A 20.5-mm-diameter tube, which allows a pixel size of 10 μm, was used. Acquisitions were made using cone beam geometry and a Feldkamp filtered back projection reconstruction algorithm was used to create the reconstructions. For the analyses of the acquired images, the CTAn analyzer software (Skyscan) was used. Three-dimensional images were reconstructed through direct volume rendering from the series of 2D projections.

Assessing mineral apposition rate by fluorescence microscopy

Retrieved calvaria specimens were transferred to processing cassettes and dehydrated to evaluate for calcium mineral apposition. Briefly, specimens were then infiltrated with increasing resin (Technovit; Heraeus Kulzer GmbH) concentrations for up to 100% for 23 days, as described by previous studies.[28] At the end of the infiltration process, specimens were polymerized in fresh resin in a light polymerization device (Exakt®; Exakt Apparatebau) and cemented to plexiglass slides. Two 300-μm sections were cut at the sagittal midline and lateral to midline of each defect. Finally, each specimen slide was thinned and polished to final sections of 50 μm. Calvaria specimens in slides were visualized using a Nikon fluorescence microscope apparatus with bright field, TRITC and FITC filters, and a Nikon

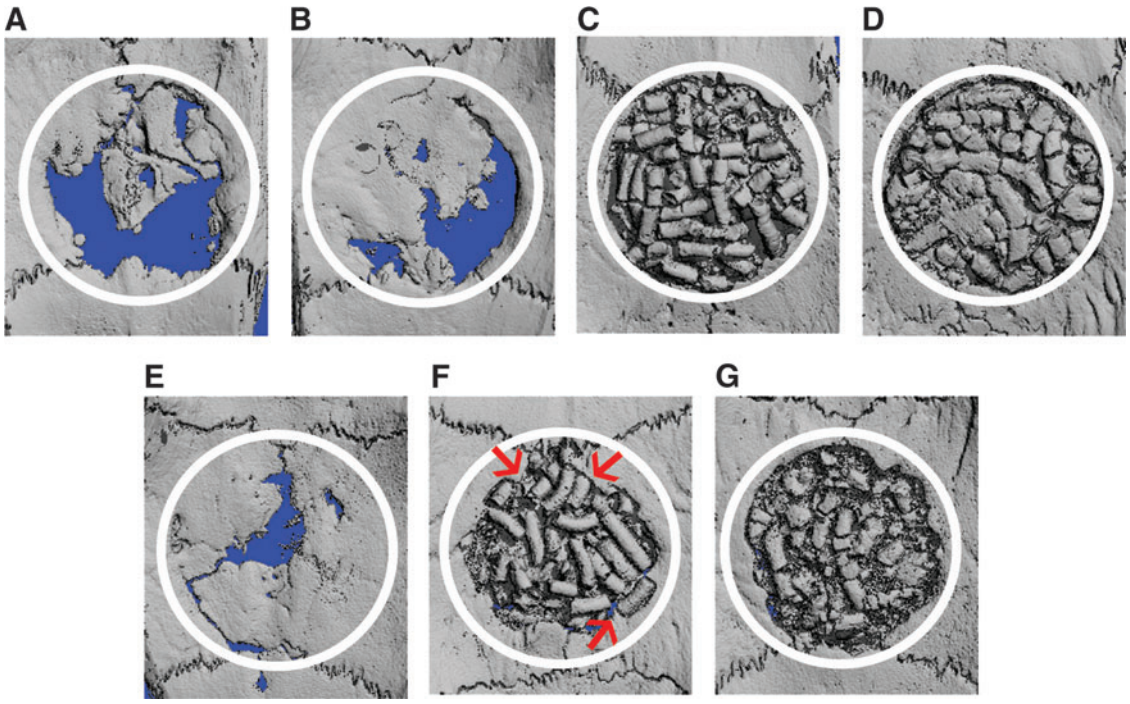

FIG. 3. Three-dimensional μCT view of calvaria defects (ventral aspect) 8 weeks postimplantation. **(A)** Empty defect–G1; **(B)** poly(lactic-co-glycolic acid) (PLGA)–G2; **(C)** HAP-GEL–G4; **(D)** titanium dioxide (TiO_2)-HAP-GEL–G5; **(E)** bone autograft–G6; **(F)** TiO_2-HAP-GEL + OD-MAPC–G7; **(G)** TiO_2-HAP-GEL + MAPC–G8. White circle represents the limits of the 8-mm-diameter defect area. Red arrows: regions of osteointegration. Color images available online at www.liebertpub.com/tea

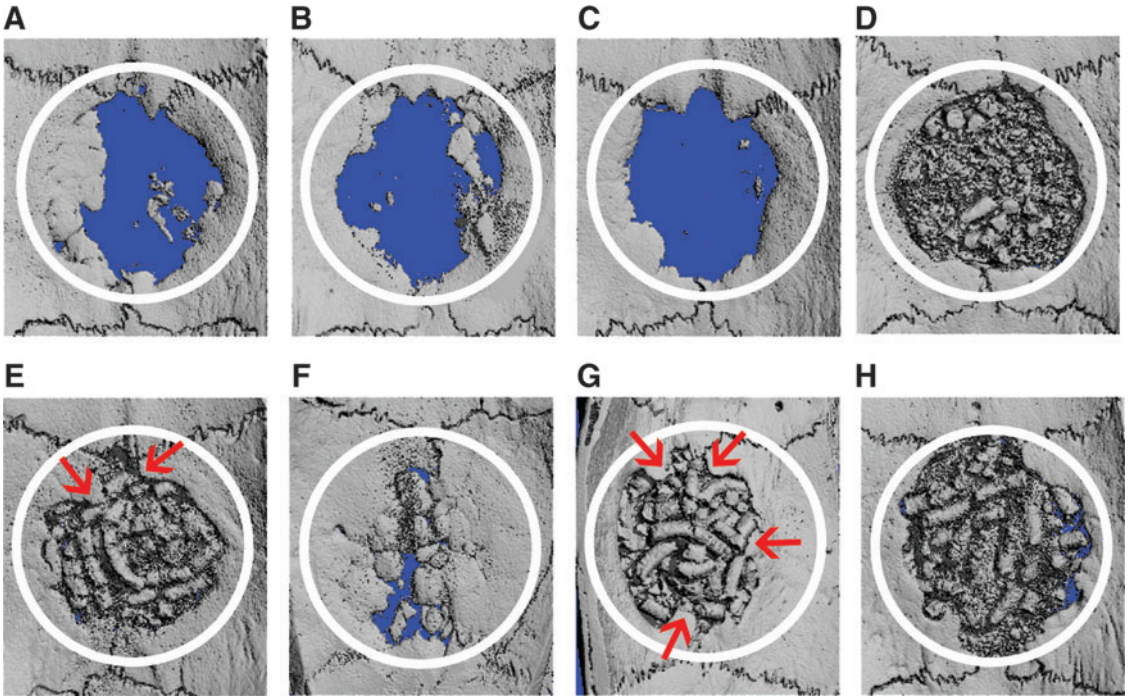

FIG. 4. Three-dimensional μCT view of calvaria defects (ventral aspect) 12 weeks postimplantation. **(A)** Empty defect–G1; **(B)** PLGA–G2; **(C)** collagen–G3; **(D)** HAP-GEL–G4; **(E)** TiO_2-HAP-GEL–G5; **(F)** bone autograft–G6; **(G, H)** TiO_2-HAP-GEL scaffold with: **(G)** OD-MAPCs–G7; and **(H)** MAPCs–G8. White circle represents the limits of the 8-mm-diameter defect area. Red arrows: regions of osteointegration. Color images available online at www.liebertpub.com/tea

Eclipse *Ti-U* digital camera. Nikon NIS Elements software was used to acquire and analyze fluorescent merged images and measure the distance between fluorescent-labeled layers where calcium mineral apposition occurred. The distance between mineral apposition layers was measured at the interface between the native bone and the implanted scaffold (INBS), both anteriorly, posteriorly, medially, and laterally with Nikon NIS Elements software tools.[27] The mean distance of the four regions was subject to statistical analysis and the overall mean distance was calculated for each rat. The mineral apposition rate (MAR) at INBS or bone healing/regeneration was calculated for 8 and 12 weeks by dividing the overall mean distance by the interlabeling period of 32 and 60 days, respectively. The MAR at the porous areas was determined by measuring the maximum length of all new bone islands in pores labeled with calcein at postsurgical day 42. All bone lengths in porous areas were summed up to get the final MAR for each animal.

Histological processing of calvaria specimens to determine new bone tissue formation and resorption activity

After fluorescence microscopy, calvaria specimen slides were stained for 15 min with Stevenel's blue and counterstained with Van Gieson for 3 min to visualize the formation of NFB tissue as described.[28] Images were acquired with an Olympus DP12 camera, which was mounted in an Olympus BX51 optical microscope (Olympus Optical Co., Ltd.). This staining procedure allowed the visualization of collagen

Table 1. *Top:* Experimental Surgical Groups with Scaffolds/Grafts Only

Cell-free scaffold groups					
G1	*G2*	*G3*	*G4*	*G5*	*G6*
Empty	PLGA	Collagen	HAP-GEL	TiO_2-HAP-GEL	Bone autograft
Cell-loaded scaffold groups					
G7			*G8*		
TiO_2-HAPGEL + 15×10^4 OD-MAPCs			TiO_2-HAPGEL + 15×10^4 MAPCs		

Bottom: Experimental surgical groups with scaffolds loaded with 10 cell aggregates/scaffold (15×10^4cells/scaffold). MAPCs: cells are at undifferentiated stage.

MAPC, multipotent adult progenitor cell; OD-MAPCs, osteogenically differentiated MAPCs; PLGA, poly(lactic-co-glycolic acid); HAP-GEL, hydroxyapatite-gelatin.

fibers and connective tissue in green or green-blue, osteoid in yellow-green, native bone in pink-light red, and NFB in intense red-purple. The medial (central) sagittal sections were chosen for bone histomorphometric analysis. Stitched images of each specimen acquired at 20× magnification were created using Adobe Photoshop CS6 (Adobe Systems, Inc.). The new bone surface area (B.Ar.) and the total area of each defect (T.Ar.) were obtained in pixels by using an image analysis system (ImageJ software version 1.46R; NIH). The NFB was calculated by determining the bone area (B.Ar./T.Ar.;%) according to standardized protocols of the American Society for Bone and Mineral Research.[29]

To evaluate for the osteoclast resorption activity, 12-week retrieved implanted HAP-GEL scaffolds were fixed, decalcified, embedded in paraffin, cut to 6-μm sections, and mounted on glass slides. The osteoclast resorption activity was evaluated using the tartaric acid-resistant acid phosphatase (TRAP) staining kit according to previous studies.[30] Blood smears were used as positive controls. Slides not treated with TRAP were used as negative controls.

Statistical analysis

Multiple student *t*-tests were performed in all experiments, except for MAR where one-way ANOVA and the Tukey-Kramer method were used for multiple statistical comparisons using JMP9 software (SAS Institute). Statistical significance was defined at $p < 0.05$.

Results

Structural strength and porosity of preimplanted HAP-GEL scaffolds

Before *in vivo* implantation in calvaria defects, the developed macroporous TiO_2-HAP-GEL scaffolds had a mean compressive strength (13.8 MPa) and porosity (34.3%) (Table 2). These properties resembled the ones found in natural calvaria bone and were superior to collagen. As a result, TiO_2-HAP-GEL scaffolds provided the strength to support the skull's structure and were deemed feasible for the rat calvaria regeneration model.

Table 2. Ultimate Compressive Strength and Porosity of the Calvaria Natural Bone Specimens and of the Preimplanted Scaffolds

	Specimens/Scaffolds		
Properties	*Calvaria bone*	*TiO_2-HAP-GEL*	*Collagen*
Compressive strength (MPa)	24.5 ± 8.3 MPa	13.8 ± 4.5 MPa*	0 ± 0.1 MPa**
Pore size (mm)	0.64 ± 0.4	1.52 ± 0.8*	N/A
Porosity (%)	22.9%	34.3%*	N/A

The preimplanted macroporous TiO_2-HAP-GEL scaffolds and the collagen scaffolds were fabricated to be shaped to the in vivo calvaria critical-size defect. Data are shown as mean ± SD of four to five independent experiments.*Denotes no statistical difference when compared to calvaria bone; **$p < 0.01$ when statistically compared to TiO_2-HAP-GEL and calvaria bone. N/A: not applicable (since collagen is radioque and cannot be analyzed by using μCT).

Retaining viable and osteogenic MAPC aggregates in scaffolds

Before loading cell aggregates into macroporous TiO_2-HAP-GEL scaffolds, MAPC aggregates were tested *in vitro* during 5 weeks of culture to confirm their osteogenic differentiation capabilities by using in TEM. Abundant mineralization with spindle-like crystals was observed in TEM of MAPC aggregate matrices (Fig. 2A). The encountered osteogenic aggregates were then loaded into the macroporous TiO_2-HAP-GEL scaffolds to assess cell viability. The majority of cells within the scaffold were found metabolically active (as indicated by red fluorescence, Fig. 2B) with scaffold macropores retaining 50–300 μm MAPC aggregates. In summary, TiO_2-HAP-GEL scaffolds not only provided the appropriate strength, but also hosted viable osteogenic MAPC aggregates. Consequently, MAPC-loaded scaffolds were feasible to be implanted in the calvaria regeneration model.

μCT analysis of calvaria defects after scaffold implantation

After 4 weeks of *in vivo* implantation, few areas of tissue growth could be observed within the defect as per 3D μCT images. (Supplementary Fig. S1A–D; Supplementary Data are available online at www.liebertpub.com/tea). All HAP-GEL-treated groups (with/without titania) had radiopacities in defects since scaffolds were composed of inherently radiopaque HAP (Supplementary Fig. S1C, D). The radiopacities associated with the above scaffolds and with natural bone had overlapping thresholds, which made it unfeasible to measure NFB using the μCT images with the current resolution of 10 μm/pixel.

Tomographic 3D images from calvaria specimens at later postimplantation times, 8 and 12 weeks, can be observed in Figures 3 and 4. At 8 weeks, the calvaria defect area was partially filled with thin layers of radiopaque bone-like tissue (RBT) in the periphery and central part of the defect in the empty (G1) and PLGA (G2) groups (Fig. 3A, B). Furthermore, TiO_2-HAP-GEL (G5) had more regions of osteointegration at INBS than HAP-GEL without titania (G4) (Fig. 3C, D), suggesting that titania additives can increase bone ingrowth in HAP-GEL biomaterial surfaces. TiO_2-HAP-GEL scaffolds with OD-MAPCs (G7) also had more osteointegration, when compared to TiO_2-HAP-GEL only (G5) (Fig. 3D, F).

At 12 weeks postimplantation, calvaria defects without a scaffold (G1), and with PLGA (G2), collagen (G3) were still < 50% filled with RBT (Fig. 4 A–C). The HAP-GEL scaffold with titanium (G5) had considerable osteointegration at INBS (red arrows in Fig. 4E) compared to titanium-free HAP-GEL (G4, Fig. 4D). Defects with cell-loaded TiO_2-HAP-GEL showed that OD-MAPCs promote greater osteointegration, bone bridging, and narrowing of the defect than undifferentiated MAPCs at 8 and 12 weeks (Fig. 3G, F, and Fig. 4G, H). As expected, the calvaria defect was nearly completely filled with RBT when an autograft (positive control) was implanted (Fig. 4F).

Mineral apposition rate

Bone regeneration was also determined by assessing the MAR at the INBS and also at the porous areas. The MAR at

INBS was evaluated 8 and 12 weeks postimplantation (between day 10 and 42 and day 10 and 70; in Fig. 5A, C) and was found significantly higher for TiO_2-enriched HAP-GEL (G5) scaffolds ($n=3$; $p<0.01$), when compared to all cell-free scaffolds, including HAP-GEL (G4). In addition, MAR with TiO_2-HAP-GEL was comparable to bone autograft at 8 weeks (G6, positive control) ($p=0.09$), but not at 12 weeks postimplantation. Therefore, TiO_2-HAP-GEL (G5) scaffolds were greatly advantageous in terms of bone healing, only comparable to the current clinical gold standard (G6). In Figure 5A and C, when OD-MAPCs were loaded into TiO_2-HAP-GEL (G7), the MAR increased significantly at the INBS ($n=3$, $p=0.0015$). This bone-healing effect did not occur when undifferentiated MAPCs (G8) were added into TiO_2-enriched scaffolds ($n=3$; $p=1.0$). In summary, the TiO_2-HAP-GEL constructs with OD-MAPCs had superior bone regeneration, only comparable to bone autograft ($n=3$; $p=0.4383$). Consistently with these findings, mineral apposition was also significantly increased in the porous areas of TiO_2-HAP-GEL scaffolds loaded with cells, but not on those without (Fig. 5B).

New bone tissue formation

After 8 and 12 weeks postimplantation on calvaria defects, NFB tissue was evaluated quantitatively and qualitatively after staining of undecalcified samples, allowing visualization of collagen fibers and connective tissue (green-blue), osteoid (yellow-green), native bone (pink-light red), and NFB (red-purple).

In Figure 5D, quantitative bone histomorphometry can be perceived and compared to a more dynamic bone histomorphometric value such as MAR at 12 weeks postimplantation (Fig. 5C). %NFB was significantly greater in TiO_2-HAP-GEL (G5) scaffolds when compared to other cell-free scaffolds (G2, G3, G4), but not with cell-loaded scaffolds TiO_2-HAP-GEL (Fig. 5D). The autograft (G6) had the least %NFB among all groups.

In qualitative studies, at lower magnification, a thin layer of NFB (red-purple) was observed in the defect of the empty and PLGA groups, G1 and G2, respectively (Fig. 6A, B). In TiO_2-HAP-GEL (G5) scaffolds, regions of osteointegration with NFB tissue (red-purple) were visualized in the INBS and inside the macroporous areas at higher magnification (Fig. 6E, E1, E2), which were not abundant in HAP-GEL (G4) (Fig. 6D, D1, D2). Unlike undifferentiated (Fig. 6G, G1, G2), OD-MAPCs with TiO_2-HAP-GEL (G5) scaffolds, showed regions of osteointegration with NFB tissue (red-purple) in the INBS (Fig. 6F, F1) and also NFB, osteoid, and collagen fibers (blue-green) forming inside the scaffold macropores (Fig. 6F2). The bone autograft (G6) had the defect largely filled with NFB, as expected (Fig. 6C).

After 12 weeks postimplantation, calcium apposition assessed by calcium fluorescence labeling (Fig. 7) and bone-specific staining (Fig. 8) confirmed that calvaria defects with TiO_2-HAP-GEL scaffolds plus OD-MAPCs (G7) were the only alloplastic constructs completely filled with newly mineralized tissue (white arrows, Fig. 7F) and NFB (black arrows, Fig. 8F), similar to the autograft-treated defect (Fig. 8H and 9H).

Resorption activity after TiO_2-HAP-GEL implantation

Ideally, scaffolds used in bone regeneration should be gradually resorbed by the osteoclasts and replaced by new bone. Therefore, after 12 weeks postimplantation, the osteoclast resorption activity at TiO_2-HAP-GEL (G5) scaffolds was assessed by TRAP staining (Fig. 9). The implanted TiO_2-HAP-GEL scaffolds exhibited regions of osteoclast resorption as indicated by the purple-maroon areas in the INBS (black arrows in Fig. 9A) like in previous studies.[31,32]

Discussion

In this study, a macroporous TiO_2-HAP-GEL scaffold for *in vivo* implantation was successfully fabricated and shaped into nonload-bearing calvaria CSD. The preimplanted TiO_2-HAP-GEL scaffolds had a final compressive strength of 13.8 ± 4.5 MPa, which is higher than the value registered for the human trabecular bone in load-bearing areas (5.6 ± 3.8 MPa in the femur and 2.22 ± 1.42 MPa in the tibia)[33,34] (Table 2). The strength of the scaffold was attributed to the diameter (700–800 μm) of the HAP-GEL trusses extruded from the syringe nozzle. Moreover, macroporous TiO_2-HAP-GEL scaffolds retained viable OD-MAPC aggregates with a 300 μm maximum size (Fig. 2B). Consequently, this tissue-engineered construct was deemed appropriate to implant in the calvaria regeneration model.

After implantation in calvaria, cell-free scaffolds did not appear to generate a radiopaque bone-like tissue after 4 weeks. The radiopacity of the HAP phase limited this evaluation. However, after 8 weeks postimplantation, TiO_2-HAP-GEL scaffolds promoted both osteointegration and filling of the 8-mm CSD at the periphery, in the interface INBS. Other cell-free scaffolds (like PLGA and collagen) produced a very thin radiopaque tissue mainly at the periphery. The scarce NFB seen in PLGA may be related to the acidity of the PLGA degradation byproducts during their fast hydrolysis, which has been reported to induce an inflammatory reaction and impair bone healing.[26] Likewise, the cell-free collagen sponge had poor NFB tissue in CSD, and thus, a modest effect on bone regeneration. This poor collagen-related effect has been recently reported at CSD in rat fibulas.[9] In this latter report, researchers found that cell-free collagen sponges have a very limited microvascular network in both fracture healing and CSD models, unlike HAP-based constructs.[9]

Results found here with the implanted cell-free TiO_2-HAP-GEL were further confirmed within the undecalcified sections with NFB-specific staining and after evaluating the MAR. The HAP-GEL without TiO_2 additives had significantly less MAR, osteointegration, and NFB in the porous areas than the HAP-GEL enriched with TiO_2. Similar observations have been reported in several different TiO_2 dental implant surfaces in *in vitro* and *in vivo* rat tibia studies.[11,35–38] The proposed mechanism of titanium-associated osteoinduction is thought to be related to hydroxyl groups and calcium ions present in TiO_2 surfaces. These hydroxyl groups may well promote adsorption of calcium-binding extracellular matrix proteins (e.g., alkaline phosphatase) and RGD-specific peptide sequences (e.g., fibronectin, bone sialoprotein).[12,39]

Interestingly, in OD-MAPCs loaded TiO_2-HAPGEL scaffolds, several areas of osteointegration were observed after 8 and 12 weeks. Furthermore, mineralized NFB tissue was seen in the pores and filled the defect length completely (Figs. 7 and 8), unlike scaffolds with undifferentiated

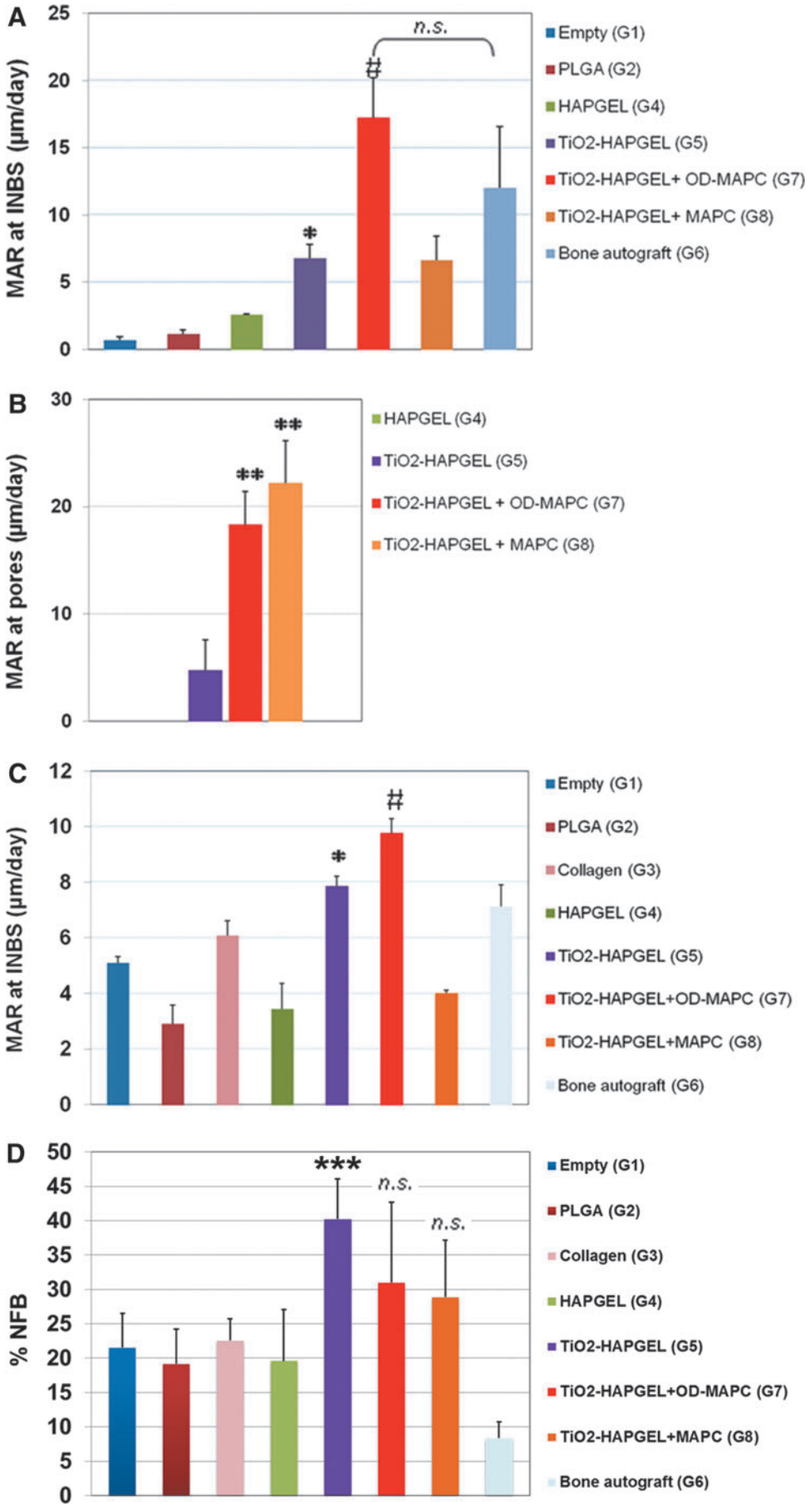

FIG. 5. Mineral apposition rate (MAR) and newly formed bone (NFB). MAR was determined at 8 weeks **(A, B)** and 12 weeks **(C)**, and NFB at 12 weeks **(D)** after implantation of scaffolds (with and without cells) and autografts. **(A, C)** At the interface native bone scaffold (INBS). **(B)** At the porous areas on the macroporous scaffolds. Data are shown as mean ± SD of three independent experiments. $*p < 0.01$ when statistically compared to cell-free scaffolds (G1, G2 and G4). $\#p < 0.05$ when statistically compared to all groups. n.s.: not significant comparison. $**p < 0.05$ when compared to cell-free scaffolds (G4 and G5). $***p < 0.05$ when compared to cell-free scaffolds and autografts (G2, G3, G4, G6), but not significant when compared to G7 and G8. Color images available online at www.liebertpub.com/tea

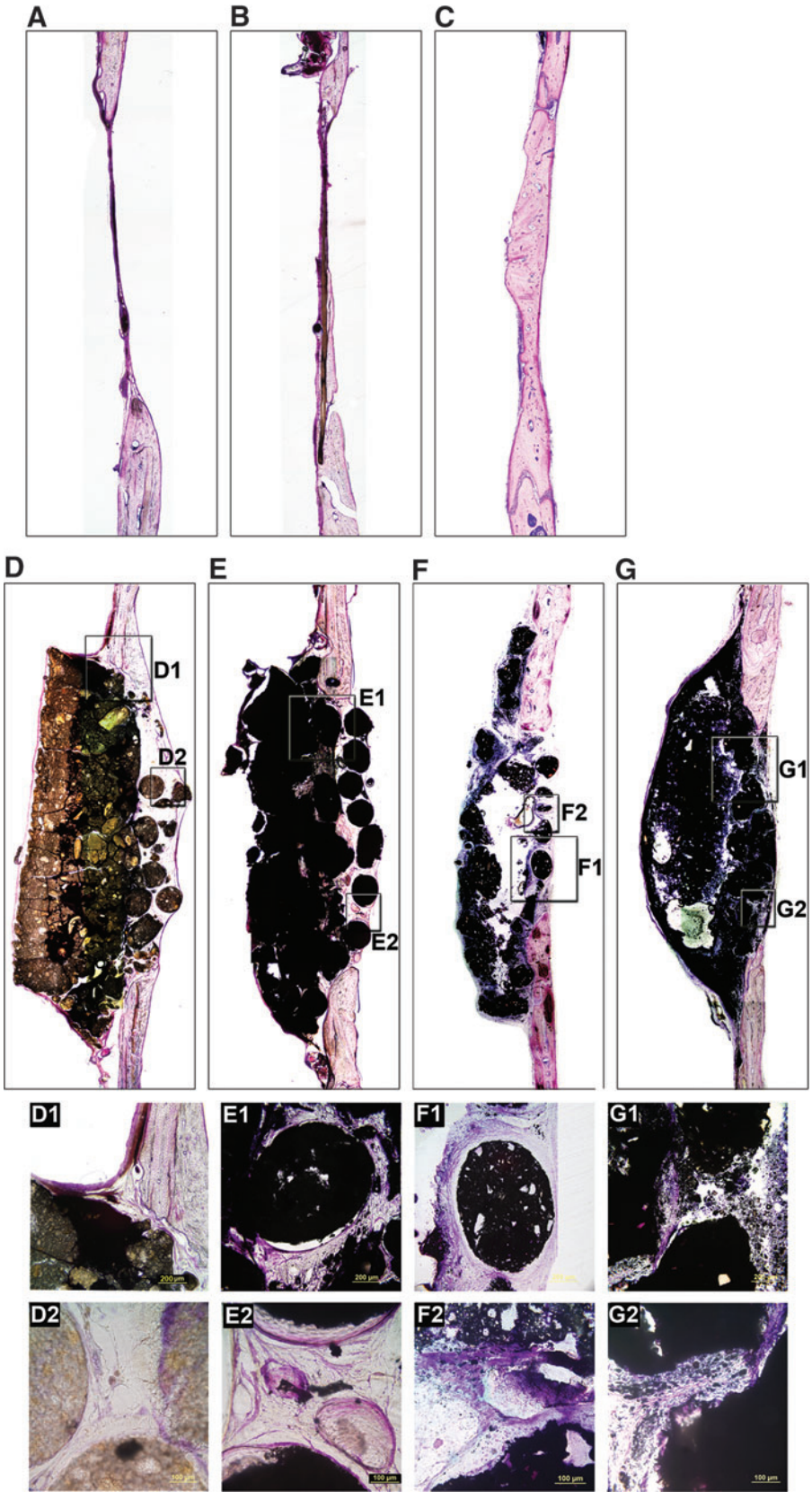

FIG. 6. NFB tissue after 8 weeks postimplantation. The following experimental groups were implanted: **(A)** G1: empty; **(B)** G2: PLGA; **(C)** G6: bone autograft; **(D)** G4: HAP-GEL; **(E)** G5: TiO_2-HAP-GEL; **(F)** G7: TiO_2-HAP-GEL + DD-MAPC; **(G)** G8: TiO_2-HAP-GEL + MAPC. All calvaria anteroposterior sagittal cross sections shown here were stained with Stevenel's blue and van Gieson. D1–G1 and D2–G2 squares were the selected regions for higher magnification shown in the inferior panel. **A–G**: Mag. 40×; D1–G1: Mag. 100×; D2–G2: Mag. 200×. Color images available online at www.liebertpub.com/tea

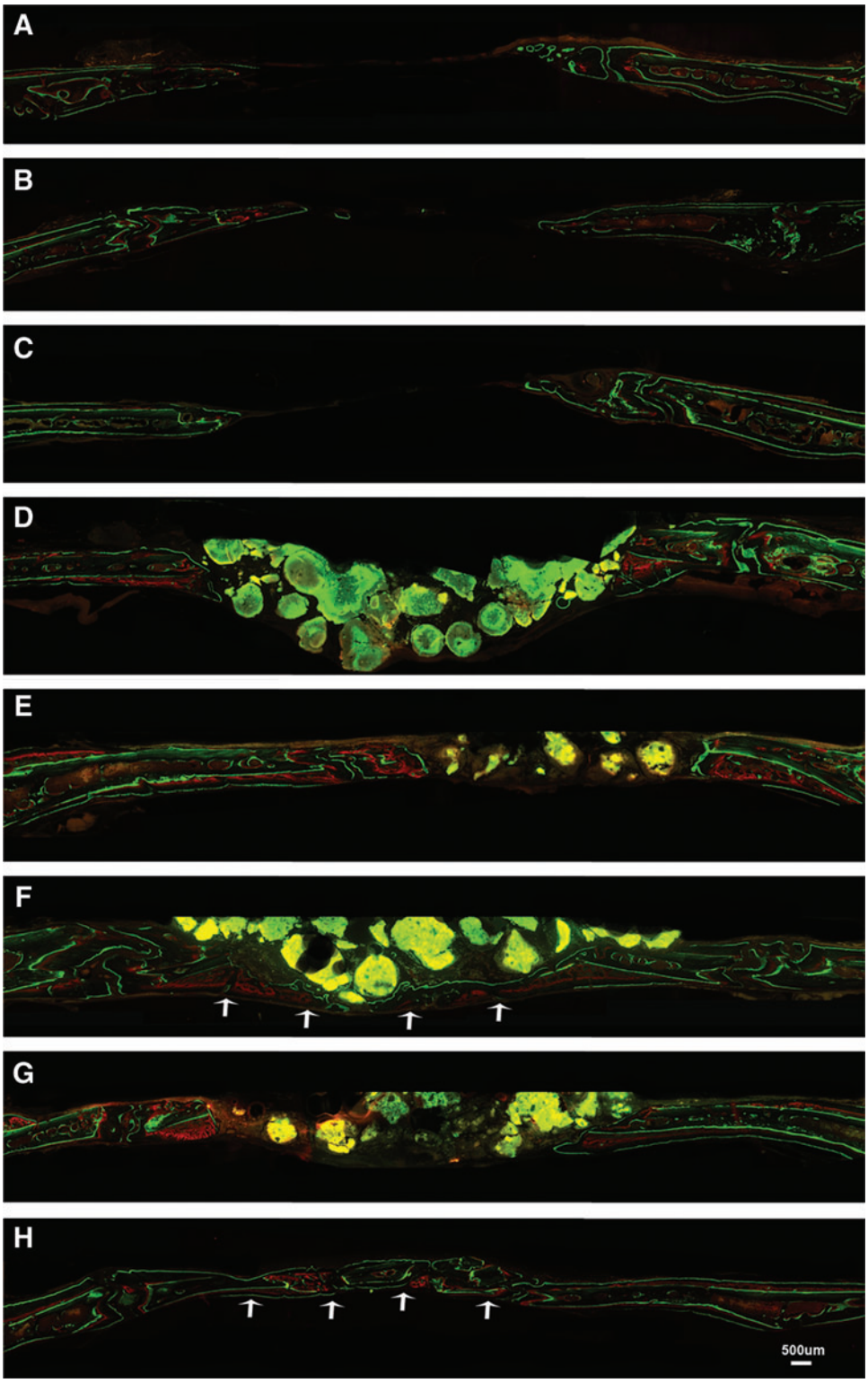

FIG. 7. Newly formed mineralized tissue in calvaria CSD after 10 days (red layers) and 70 days (green layers) postimplantation of scaffolds/cells and autografts. The following experimental groups were implanted: **(A)** G1: empty; **(B)** G2: PLGA; **(C)** G3: collagen; **(D)** G4: HAP-GEL; **(E)** G5: TiO_2-HAP-GEL; **(F)** G7: TiO_2-HAP-GEL + DD-MAPC; **(G)** G8: TiO_2-HAP-GEL + MAPC; **(H)** G6: bone autograft. All represent calvaria anteroposterior midsagittal cross sections labeled *in vivo* with Alizarin Red (day 10) and calcein (day 60). White arrows indicate the mineralized NFB tissue filling the CSD area. Mag. 40×. Color images available online at www.liebertpub.com/tea

MAPCs. In addition, bone regeneration by MAR at the INBS was significantly greater in differentiated than in undifferentiated MAPCs. This dichotomy between *in vivo* bone-healing effects of undifferentiated and osteogenically differentiated adult stem cells has also been recently reported.[20] In this latter report, osteogenically differentiated adipose-derived MSCs induced significantly more bone regeneration than undifferentiated cells after 6 weeks in calvaria CSD.[20] Previous to implantation, the differentiation conditions for committing MAPCs to osteoprogenitor cells *in vitro* have required long culture periods, as in differentiation of human embryonic stem cells into mesenchymal

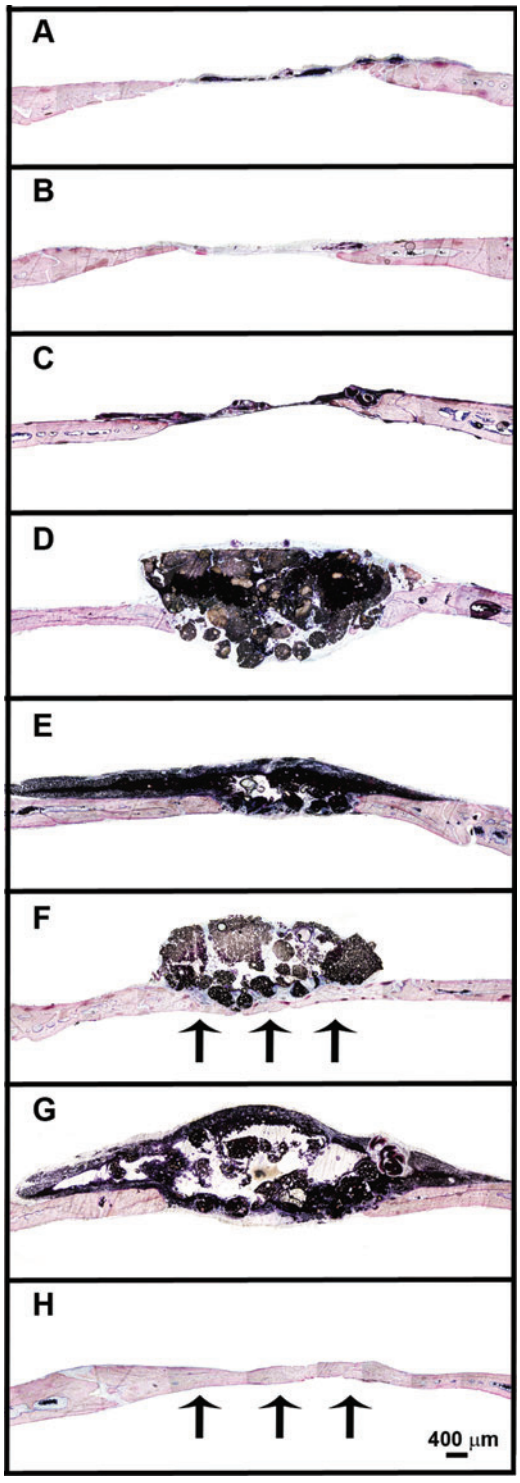

FIG. 8. NFB tissue in calvaria CSD 12 weeks post-implantation of scaffolds/cells and autografts. The following experimental groups were implanted: **(A)** G1: empty; **(B)** G2: PLGA; **(C)** G3: collagen; **(D)** G4: HAP-GEL; **(E)** G5: TiO_2-HAP-GEL; **(F)** G7: TiO_2-HAP-GEL + DD-MAPC; **(G)** G8: TiO_2-HAP-GEL + MAPC; **(H)** G6: bone autograft. All calvaria anteroposterior midsagittal cross sections shown here were stained with Stevenel's blue and van Gieson. Black arrows indicate the NFB tissue filling the CSD area. Mag. 40×. Color images available online at www.liebertpub.com/tea

precursors.[5,40–42] However, to satisfy the demand of high osteoprogenitor cell numbers to regenerate large skeletal defects via a tissue-engineered approach, novel aggregate culture conditions were used here to assure a consistent MAPC osteogenic differentiation on a large scale.[17] More than 1000 progenitor cells/cm^3 have been required for bone healing to occur.[43] Here 15×10^4 cells were scaffold-seeded (surpassing the required number) and contributed to the complete healing observed in calvaria defects.

Significant differences in MAR were found at 8 and 12 weeks between TiO_2-HAP-GEL with OD-MAPCs and all other groups (excluding the autograft group, Fig. 5A–C). Despite the significance of the *in vivo* outcomes, a larger sample size may be necessary in future studies ($n>3$). The sole contribution of OD-MAPCs to the newly engineered TiO_2-HAP-GEL scaffold is debatable because new bone formation assessed by red-purple color in bone histomorphometry indicated that bone healing in defects with TiO_2-HAP-GEL is similar when comparing without and with MAPC/OD-MAPCs (Fig. 5D). However, this histomorphometry method based on a very similar range of colors (pink, red, purple) requires a subjective analysis, which has its limitations.[29,44] This color-method did not allow us to evaluate properly the new lamellar bone in the trabeculae and Haversian system, particularly on the autograft group, which reflected on its very low values of bone healing. On the contrary, MAR is a more dynamic and objective bone histomorphometric marker that considers the time-course bone remodeling activity, and relies on two very distinct fluorescent colors (red versus green).[27,29] As such, high MAR values (6–8 μm/day) were expected for the autograft.

In *in vivo* reports using allogeneic cell sources, the recruitment of host osteoprogenitor cells by allogeneic adult stem cells similar to MAPCs has been documented and found crucial for bioengineering new bone.[45] In addition, allogeneic adult stem cells can be defect-retained for more than 9 weeks following implantation,[46] although these findings are species dependent.[45] Species-specific differences do exist in the regulation of the immunity, in the mechanism of bone formation, or in the site of implantation. In recent literature, higher ratios of M2/M1 macrophages concomitantly with an absence of a foreign body response have been found with scaffolds having 30–40-μm pores when compared to hosts with nonporous implants.[47] In this study, TiO_2-HAP-GEL scaffolds had 34% porosity with 1.52 ± 0.8-mm pores and were not engineered *in vitro* as in other studies[48] reporting a M1 predominant immune response (to engineered *in vitro* matrices); therefore, we would expect to have no foreign body response and a predominant M2 macrophage activity. Moreover, human MAPCs were recently found safe for clinical trials for treatment of graft-versus-host disease (ClinicalTrials.gov NCT00677859, NCT00677222). Despite these facts, we believe that it would be beneficial to assess the M1/M2 host response in future studies particularly when using allogeneic (nonautologous) MAPC transplants.[48,49] The immune rejection mechanism can start between day 3 and day 8 after implantation of allogeneic stem cells.[45] In our previous studies, we found no rejection-associated tissue necrosis or mixed lymphocytic reaction 10 days after implantation of OD-MAPCs.[5] In fact, OD-MAPCs were found growing in HAP porous areas between day 4 and 10 in calvaria defects.

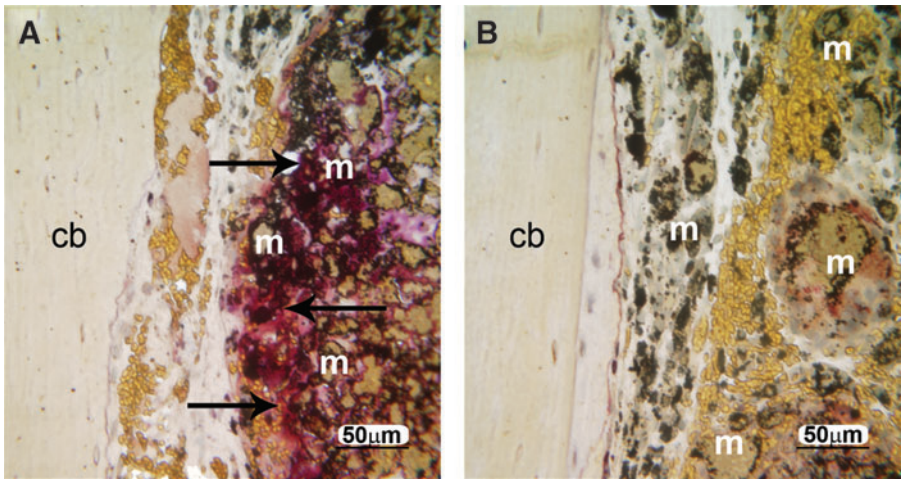

FIG. 9. The resorptive activity of osteoclasts in TiO_2-HAP-GEL scaffolds (in black arrows) on calvaria CSD 12 weeks postimplantation, after tartaric acid-resistant acid phosphatase (TRAP) staining. **(A)** TRAP treatment. **(B)** No TRAP treatment (negative control). cb: calvaria bone; m: material leftover from TiO_2-HAP-GEL scaffolds; Mag. 400×. Color images available online at www.liebertpub.com/tea

Clinical advantages of HAP-based constructs for bone regeneration are many and include, a decreased potential for infection and elimination of the necessity of a donor site.[50] Postsurgical complications are minor and are generally associated with the slow HAP degradation.[31,32,50] In this study, the TiO_2-HAP-GEL scaffold was degraded into smaller pieces after 12 weeks, and the host TRAP activity was abundantly present surrounding the biomaterials (Fig. 9). However, the nonporous base used (for the scaffold retention) may take more time to degrade, particularly on HAP-GEL scaffolds (without TiO_2), since these inherently possess greater amount of the aminosilane binder or crosslinker.[6] In addition, higher concentrations of the aminosilane may reduce the porosity and limit the migration of osteoprogenitor cells residing on the dorsal and ventral periosteum in this calvaria model.[6,51]

The formation of a microvascular network in porous scaffolds was not the main goal of this study, and therefore, it was not thoroughly evaluated. However, in the future, these HAP-GEL constructs may require loading of endothelial progenitor cells to generate microvascularization and promote a faster regeneration.[9]

In conclusion, the fabrication of a rigid macroporous TiO_2-enriched HAP-GEL scaffold was found feasible for bone regeneration applications in calvaria defects. After 12 weeks postimplantation, TiO_2-HAP-GEL scaffolds loaded with OD-MAPCs promoted osteointegration, NFB in the macroporous areas and significantly enhanced bone regeneration. Also, TiO_2-HAP-GEL scaffolds had greater bone regeneration than other cell-free scaffolds (PLGA, collagen, and HAP-GEL). Finally, constructs with TiO_2-HAP-GEL scaffolds and OD-MAPCs had a greater bone healing than the cell-free TiO_2-HAP-GEL with complete closure of the defect. Thus, TiO_2-HAP-GEL constructs with OD-MAPCs can be applied in craniofacial bone regeneration models (e.g., calvaria) to enhance bone healing and regeneration. These constructs will need further testing in load-bearing models.

Acknowledgments

We would like to acknowledge Mr. Michael Vick, Dr. Weihan Hsieh, and Dr. Faiz Malabari for their surgical assistance and to Professor Eric Everett and Dr. Brandon Frederick for technical support with μCT imaging. Also, our thanks go to Mrs. Sandra Horton at the North Carolina State University for processing calvaria tissue specimens and to Mrs. Victoria Madden at the UNC Microscopy Services Laboratory for processing *in vitro* cell matrices for electron microscopy. João Ferreira was supported by the doctoral fellowship of FCT-Portuguese Foundation for Science and Technology (SFRH/BD/36841/2007). This work was supported, in part, by grants from the NIH/NIDCR (K08DE018695), NC Biotech Center, American Association for Orthodontist Foundation awarded to C.-C. Ko. All authors reported no conflict of interests. Dr. Ko is the cofounder of Ironwood Materials Science, Inc. This work, however, was not supported by any company and does not relate to any commercialized products.

Disclosure Statement

The authors report that no competing financial interests exist.

References

1. United States Bone and Joint Decade. *The Burden of Musculoskeletal Diseases in the United States*, 2008. www.boneandjointburden.org
2. Bueno, E.M., and Glowacki, J. Cell-free and cell-based approaches for bone regeneration. Nat Rev Rheumatol **5,** 685, 2009.
3. Giannoudis, P.V., Dinopoulos, H., and Tsiridis, E. Bone substitutes: an update. Injury **36 Suppl 3,** S20, 2005.
4. Lucarelli, E., Donati, D., Cenacchi, A., and Fornasari, P.M. Bone reconstruction of large defects using bone marrow derived autologous stem cells. Transfus Apher Sci **30,** 169, 2004.
5. Ferreira, J.R., Hirsch, M.L., Zhang, L., Park, Y., Samulski, R.J., Hu, W.S., and Ko, C.C. Three-dimensional multipotent progenitor cell aggregates for expansion, osteogenic differentiation and 'in vivo' tracing with AAV vector serotype 6. Gene Ther **20,** 158, 2012.
6. Luo, T.M., Ko, C.C., Chiu, C.K., Lloyd, J., and Huh, U. Aminosilane as an effective binder for hydroxyapatite-gelatin nanocomposites. J Sol-Gel Sci Technol **53,** 459, 2010.
7. Chiu, C.K., Ferreira, J., Luo, T.J., Geng, H., Lin, F.C., and Ko, C.C. Direct scaffolding of biomimetic hydroxyapatite-gelatin nanocomposites using aminosilane cross-linker for bone regeneration. J Mater Sci Mater Med **23,** 2115, 2012.

8. Kon, E., Muraglia, A., Corsi, A., Bianco, P., Marcacci, M., Martin, I., Boyde, A., Ruspantini, I., Chistolini, P., Rocca, M., Giardino, R., Cancedda, R., and Quarto, R. Autologous bone marrow stromal cells loaded onto porous hydroxyapatite ceramic accelerate bone repair in critical-size defects of sheep long bones. J Biomed Mater Res **49,** 328, 2000.
9. Chandrasekhar, K.S., Zhou, H., Zeng, P., Alge, D., Li, W., Finney, B.A., Yoder, M.C., and Li, J. Blood vessel wall-derived endothelial colony-forming cells enhance fracture repair and bone regeneration. Calcif Tissue Int **89,** 347, 2011.
10. Thein-Han, W., and Xu, H.H. Collagen-calcium phosphate cement scaffolds seeded with umbilical cord stem cells for bone tissue engineering. Tissue Eng Part A **17,** 2943, 2011.
11. Olivares-Navarrete, R., Hyzy, S.L., Park, J.H., Dunn, G.R., Haithcock, D.A., Wasilewski, C.E., Boyan, B.D., and Schwartz, Z. Mediation of osteogenic differentiation of human mesenchymal stem cells on titanium surfaces by a Wnt-integrin feedback loop. Biomaterials **32,** 6399, 2011.
12. Ellingsen, J.E. A study on the mechanism of protein adsorption to TiO2. Biomaterials **12,** 593, 1991.
13. Han, X., Liu, H., Wang, D., Su, F., Zhang, Y., Zhou, W., Li, S., and Yang, R. Alveolar bone regeneration around immediate implants using an injectable nHAC/CSH loaded with autogenic blood-acquired mesenchymal progenitor cells: an experimental study in the dog mandible. Clin Implant Dent Relat Res, 2011. [Epub ahead of print]; DOI: 10.1111/j.1708-8208.2011.00373.x.
14. Ulloa-Montoya, F., Kidder, B.L., Pauwelyn, K.A., Chase, L.G., Luttun, A., Crabbe, A., Geraerts, M., Sharov, A.A., Piao, Y., Ko, M.S., Hu, W.S., and Verfaillie, C.M. Comparative transcriptome analysis of embryonic and adult stem cells with extended and limited differentiation capacity. Genome Biol **8,** R163, 2007.
15. Subramanian, K., Geraerts, M., Pauwelyn, K.A., Park, Y., Owens, D.J., Muijtjens, M., Ulloa-Montoya, F., Jiang, Y., Verfaillie, C.M., and Hu, W.S. Isolation procedure and characterization of multipotent adult progenitor cells from rat bone marrow. Methods Mol Biol **636,** 55, 2010.
16. Park, Y., Subramanian, K., Verfaillie, C.M., and Hu, W.S. Expansion and hepatic differentiation of rat multipotent adult progenitor cells in microcarrier suspension culture. J Biotechnol **150,** 131, 2010.
17. Subramanian, K., Park, Y., Verfaillie, C.M., and Hu, W.S. Scalable expansion of multipotent adult progenitor cells as three-dimensional cell aggregates. Biotechnol Bioeng **108,** 364, 2011.
18. Reyes, M., Lund, T., Lenvik, T., Aguiar, D., Koodie, L., and Verfaillie, C.M. Purification and *ex vivo* expansion of postnatal human marrow mesodermal progenitor cells. Blood **98,** 2615, 2001.
19. Roobrouck, V.D., Clavel, C., Jacobs, S.A., Ulloa-Montoya, F., Crippa, S., Sohni, A., Roberts, S.J., Luyten, F.P., Van Gool, S.W., Sampaolesi, M., Delforge, M., Luttun, A., and Verfaillie, C.M. Differentiation potential of human postnatal mesenchymal stem cells, mesoangioblasts, and multipotent adult progenitor cells reflected in their transcriptome and partially influenced by the culture conditions. Stem Cells **29,** 871, 2011.
20. Di Bella, C., Farlie, P., and Penington, A.J. Bone regeneration in a rabbit critical-sized skull defect using autologous adipose-derived cells. Tissue Eng Part A **14,** 483, 2008.
21. Chang, M.C., Ko, C.C., and Douglas, W.H. Preparation of hydroxyapatite-gelatin nanocomposite. Biomaterials **24,** 2853, 2003.
22. Dean, D., Wolfe, M.S., Ahmad, Y., Totonchi, A., Chen, J.E., Fisher, J.P., Cooke, M.N., Rimnac, C.M., Lennon, D.P., Caplan, A.I., Topham, N.S., and Mikos, A.G. Effect of transforming growth factor beta 2 on marrow-infused foam poly(propylene fumarate) tissue-engineered constructs for the repair of critical-size cranial defects in rabbits. Tissue Eng **11,** 923, 2005.
23. Kalish, B.P., Schuster, G.S., Peacock, M.E., Cuenin, M.F., Swiec, G.D., Potter, B.J., Buxton, T.B., and McPherson, J.C., 3rd. Influence of matrix-suspended demineralized bone on osseous repair using a critical-sized defect in the rat (Rattus norvegicus) calvarium. J Oral Implantol **34,** 83, 2008.
24. Patel, Z.S., Young, S., Tabata, Y., Jansen, J.A., Wong, M.E., and Mikos, A.G. Dual delivery of an angiogenic and an osteogenic growth factor for bone regeneration in a critical size defect model. Bone **43,** 931, 2008.
25. Miguez, P.A., Terajima, M., Nagaoka, H., Mochida, Y., and Yamauchi, M. Role of glycosaminoglycans of biglycan in BMP-2 signaling. Biochem Biophys Res Commun **405,** 262, 2011.
26. Kim, I.A., and Rhee, S.H. Effects of poly(lactic-co-glycolic acid) (PLGA) degradability on the apatite-forming capacity of electrospun PLGA/SiO(2)-CaO nonwoven composite fabrics. J Biomed Mater Res Part B Appl Biomater **93,** 218, 2010.
27. Rodriguez, R., Kondo, H., Nyan, M., Hao, J., Miyahara, T., Ohya, K., and Kasugai, S. Implantation of green tea catechin alpha-tricalcium phosphate combination enhances bone repair in rat skull defects. J Biomed Mater Res Part B Appl Biomater **98B,** 263, 2011.
28. Maniatopoulos, C., Rodriguez, A., Deporter, D.A., and Melcher, A.H. An improved method for preparing histological sections of metallic implants. Int J Oral Maxillofac Implants **1,** 31, 1986.
29. Parfitt, A.M., Drezner, M.K., Glorieux, F.H., Kanis, J.A., Malluche, H., Meunier, P.J., Ott, S.M., and Recker, R.R. Bone histomorphometry: standardization of nomenclature, symbols, and units. Report of the ASBMR Histomorphometry Nomenclature Committee. J Bone Miner Res **2,** 595, 1987.
30. Parkinson, I.H., Parsons, A.M., and Moore, R.J. The histochemical localization of osteoclasts in EDTA decalcified bone. J Histotechnol **13,** 189, 1990.
31. Monchau, F., Lefevre, A., Descamps, M., Belquin-myrdycz, A., Laffargue, P., and Hildebrand, H.F. *In vitro* studies of human and rat osteoclast activity on hydroxyapatite, beta-tricalcium phosphate, calcium carbonate. Biomol Eng **19,** 143, 2002.
32. Ramaswamy, Y., Haynes, D.R., Berger, G., Gildenhaar, R., Lucas, H., Holding, C., and Zreiqat, H. Bioceramics composition modulate resorption of human osteoclasts. J Mater Sci Mater Med **16,** 1199, 2005.
33. Kuhn, J.L., Goldstein, S.A., Ciarelli, M.J., and Matthews, L.S. The limitations of canine trabecular bone as a model for human: a biomechanical study. J Biomech **22,** 95, 1989.
34. Rohl, L., Larsen, E., Linde, F., Odgaard, A., and Jorgensen, J. Tensile and compressive properties of cancellous bone. J Biomech **24,** 1143, 1991.
35. Schwartz, Z., Olivares-Navarrete, R., Wieland, M., Cochran, D.L., and Boyan, B.D. Mechanisms regulating increased production of osteoprotegerin by osteoblasts cultured on microstructured titanium surfaces. Biomaterials **30,** 3390, 2009.
36. Morinaga, K., Kido, H., Sato, A., Watazu, A., and Matsuura, M. Chronological changes in the ultrastructure of titanium-bone interfaces: analysis by light microscopy, transmission electron microscopy, and micro-computed tomography. Clin Implant Dent Relat Res **11,** 59, 2009.

37. Masuda, T., Salvi, G.E., Offenbacher, S., Felton, D.A., and Cooper, L.F. Cell and matrix reactions at titanium implants in surgically prepared rat tibiae. Int J Oral Maxillofac Implants **12,** 472, 1997.
38. Okamatsu, K., Kido, H., Sato, A., Watazu, A., and Matsuura, M. Ultrastructure of the interface between titanium and surrounding tissue in rat tibiae—a comparison study on titanium-coated and -uncoated plastic implants. Clin Implant Dent Relat Res **9,** 100, 2007.
39. Pham, M.T., Reuther, H., and Maitz, M.F. Native extracellular matrix coating on Ti surfaces. J Biomed Mater Res Part A **66,** 310, 2003.
40. Arpornmaeklong, P., Brown, S.E., Wang, Z., and Krebsbach, P.H. Phenotypic characterization, osteoblastic differentiation, and bone regeneration capacity of human embryonic stem cell-derived mesenchymal stem cells. Stem Cells Dev **18,** 955, 2009.
41. Arpornmaeklong, P., Wang, Z., Pressler, M.J., Brown, S.E., and Krebsbach, P.H. Expansion and characterization of human embryonic stem cell-derived osteoblast-like cells. Cell Reprogram **12,** 377, 2010.
42. Olivier, E.N., and Bouhassira, E.E. Differentiation of human embryonic stem cells into mesenchymal stem cells by the "raclure" method. Methods Mol Biol **690,** 183, 2011.
43. Hernigou, P., Mathieu, G., Poignard, A., Manicom, O., Beaujean, F., and Rouard, H. Percutaneous autologous bone-marrow grafting for nonunions: influence of the number and concentration of progenitor cells. J Bone Joint Surg Am **87,** 1430, 2005.
44. Dieckmann, M., Beil, F.T., Mueller, B., Bartelt, A., Marshall, R.P., Koehne, T., Amling, M., Ruether, W., Cooper, J.A., Humphries, S.E., Herz, J., and Niemeier, A. Human apolipoprotein E isoforms differentially affect bone mass and turnover *in vivo*. J Bone Miner Res **28,** 236, 2013.
45. Tasso, R., Augello, A., Boccardo, S., Salvi, S., Carida, M., Postiglione, F., Fais, F., Truini, M., Cancedda, R., and Pennesi, G. Recruitment of a host's osteoprogenitor cells using exogenous mesenchymal stem cells seeded on porous ceramic. Tissue Eng Part A **15,** 2203, 2009.
46. De Kok, I.J., Peter, S.J., Archambault, M., van den Bos, C., Kadiyala, S., Aukhil, I., and Cooper, L.F. Investigation of allogeneic mesenchymal stem cell-based alveolar bone formation: preliminary findings. Clin Oral Implants Res **14,** 481, 2003.
47. Madden, L.R., Mortisen, D.J., Sussman, E.M., Dupras, S.K., Fugate, J.A., Cuy, J.L., Hauch, K.D., Laflamme, M.A., Murry, C.E., and Ratner, B.D. Proangiogenic scaffolds as functional templates for cardiac tissue engineering. Proc Natl Acad Sci U S A **107,** 15211, 2010.
48. Lyons, F.G., Al-Munajjed, A.A., Kieran, S.M., Toner, M.E., Murphy, C.M., Duffy, G.P., and O'Brien, F.J. The healing of bony defects by cell-free collagen-based scaffolds compared to stem cell-seeded tissue engineered constructs. Biomaterials **31,** 9232, 2010.
49. Brown, B.N., Ratner, B.D., Goodman, S.B., Amar, S., and Badylak, S.F. Macrophage polarization: an opportunity for improved outcomes in biomaterials and regenerative medicine. Biomaterials **33,** 3792, 2012.
50. Kent, J.N., Zide, M.F., Kay, J.F., and Jarcho, M. Hydroxylapatite blocks and particles as bone graft substitutes in orthognathic and reconstructive surgery. J Oral Maxillofac Surg **44,** 597, 1986.
51. Gupta, A., Lobocki, C., Malhotra, G., and Jackson, I.T. Comparison of osteogenic potential of calvarial bone dust, bone fragments, and periosteum. J Craniofac Surg **20,** 1995, 2009.

Address correspondence to:
João R. Ferreira, DDS, PhD
Matrix and Morphogenesis Section
LCDB, NIDCR
30 Convent Dr., Room 429
Bethesda, MD 20892

E-mail: andraderequicj@nidcr.nih.gov

Ching-Chang Ko, DDS, PhD
275 Brauer Hall
School of Dentistry
UNC-Chapel Hill
Orthodontics
CB 7454
Chapel Hill, NC 27599

E-mail: koc@dentistry.unc.edu

Received: August 25, 2012
Accepted: March 8, 2013
Online Publication Date: April 12, 2013